



ISSN: 2617-6548

URL: [www.ijirss.com](http://www.ijirss.com)



## Governing factors – surface integrity correlations and optimizations of diamond burnishing process of chromium-nickel austenitic stainless steels of the 18/8 type

 Mariana Ichkova<sup>1\*</sup>,  Kalin Anastasov<sup>1,2</sup>,  Petya Daskalova<sup>1</sup>

<sup>1</sup>Department of Material Science and Mechanics of Materials, Technical University of Gabrovo, 5300 Gabrovo, Bulgaria.

<sup>2</sup>Center of competence "Smart mechatronic, eco-and energy-saving systems and technologies", Technical University of Gabrovo, 5300 Gabrovo, Bulgaria.

Corresponding author: Mariana Ichkova (Email: [ichkova@tugab.bg](mailto:ichkova@tugab.bg))

### Abstract

Diamond burnishing (DB), based on cold severe surface plastic deformation, is a method for modifying the surface layers of metal components in order to improve surface integrity (SI). This study aims to establish explicit correlations between the five main governing factors (burnishing force, feed rate, burnishing velocity, diamond radius, and number of passes) of DB 304 stainless steel and the main SI characteristics, including average roughness parameter Ra, shape roughness parameters skewness and kurtosis, and microhardness. DB was undertaken on a CNC lathe using flood lubrication and a one-way working scheme. A burnisher with elastic contact and a spherical-ended polycrystalline diamond insert was used. The steel, with a hardness of 250 HB, was tested in its as-received state. An experiment with a second-order composition plan, analysis of variance (ANOVA), and regression analyses was employed. The significance of the variables in the regression models was assessed using various methods to determine the influences of the governing factors and the interactions between them on the characteristics of SI. Finally, various optimizations were conducted depending on the functional purpose of the diamond-burnished surface using a non-dominated sorting genetic algorithm and QStatLab software.

**Keywords:** Austenitic stainless steel, Diamond burnishing, Optimizations, Surface integrity.

**DOI:** 10.53894/ijirss.v8i3.7450

**Funding:** This research was funded by the European Regional Development Fund under the Operational Program "Scientific Research, Innovation and Digitization for Smart Transformation 2021–2027", Project CoC "SmartMechatronics, Eco- and Energy Saving Systems and Technologies", BG16RFPR002-1.014-0005.

**History: Received:** 14 April 2025 / **Revised:** 19 May 2025 / **Accepted:** 21 May 2025 / **Published:** 28 May 2025

**Copyright:** © 2025 by the authors. This article is an open access article distributed under the terms and conditions of the Creative Commons Attribution (CC BY) license (<https://creativecommons.org/licenses/by/4.0/>).

**Competing Interests:** The authors declare that they have no competing interests.

**Authors' Contributions:** All authors contributed equally to the conception and design of the study. All authors have read and agreed to the published version of the manuscript.

**Transparency:** The authors confirm that the manuscript is an honest, accurate, and transparent account of the study; that no vital features of the study have been omitted; and that any discrepancies from the study as planned have been explained. This study followed all ethical practices during writing.

**Publisher:** Innovative Research Publishing

## 1. Introduction

The global stainless steel market size is estimated at US\$117.63 billion in 2023, and is expected to grow at a compound annual growth rate of 6.7% through 2030 [1]. Austenitic steels are the most important class of stainless steels in terms of scale of distribution and universality of use [1, 2]. Most of them are chromium-nickel stainless steels due to their favorable combination of properties: superior general corrosion resistance, good machinability by both cutting and plastic deformation, and good weldability. The most common grade is 304, which is of the 18/8 type (about 18 wt% chromium and 8 wt% nickel). Besides their tendency toward intergranular corrosion in the temperature range 500-700 °C, another disadvantage of these steels is their insufficient hardness and strength. Overcoming this drawback is achieved by bulk cold working [3, 4] or by modifying the surface layers (SL) through low-temperature nitriding and/or carburizing to form an S-phase [5, 6] surface cold working [7, 8] or a combination of both [9, 10]. The first approach is mainly limited to blanks and details made of sheet material, while the modification of the surface layers is significantly more promising, readying these layers for exposure to external influences of various natures, including aggressive ones such as seawater or other chemically active environments.

It is known [11] that the operating behavior (wear, fatigue, corrosion) of the details is directly correlated with the complex state of SL, known as surface integrity (SI), immediately after the respective finishing. Texture, microhardness, residual stresses, and microstructure (phases, shape, and grain orientation) influence the tribological behavior, fatigue strength, and corrosion resistance of the respective metal component [12-18].

An effective approach to improve SI is surface cold working (SCW) [19], which can be dynamic (shot peening [20]) surface mechanical attrition treatment [21], etc.) or static. In static SCW (also called burnishing), a hard and smooth deforming element is pressed with a constant static force against the surface being machined and moves with respect to it. Thus, the SL deforms plastically at a temperature below the recrystallization temperature of the material being processed. As a result, the roughness decreases dramatically, the surface microhardness increases significantly, beneficial residual compressive stresses are introduced into the surface and nearby subsurface layers, and the microstructure in these layers is modified toward grain refinement and orientation [22].

When the deforming element rubs along the workpiece, entailing sliding friction, the static SCW is known as slide burnishing (SB) [23]. SB can be realized with a non-diamond [24-26] or diamond [27-29] deforming element. In the second case, SB is called diamond burnishing (DB), which was introduced in 1962 by General Electric [30] to improve the SI of metal components. DB is a simple and effective finishing process and its main advantage over roller burnishing [31] is the significantly simpler equipment. An experimental comparison between DB and deep rolling showed the advantage of DB in terms of SI characteristics and fatigue behavior [32].

Over the past six decades, DB has established itself as an effective finishing technique for structural [33] tool [34] and stainless [35, 36] steels, high-strength titanium [37] and aluminum [38, 39] alloys, bronze [40] and other alloys.

The main governing factors of the DB process are the following: radius ( $r$ ) of the spherical (diameter of the cylindrical) diamond deforming element, burnishing force ( $F_b$ ), feed rate ( $f$ ), burnishing velocity ( $v$ ), and number of passes ( $n$ ). These factors are independent, but some of them act together on particular surface integrity (SI) characteristics, whether to reinforce each other or act in opposition. Hence, all governing factors (as well as the interactions between them) on SI must be considered in order to design an efficient and economical DB process to produce the desired surface properties.

Recent studies have examined the influence of the DB governing factors on the SI characteristics [11, 29, 41-46] and operating behavior (corrosion, wear, fatigue) [10, 11, 13, 18, 22, 29, 35, 41] of specimens made from chromium-nickel austenitic steels. Given the established correlations between SI and operating behavior [11, 47] it is very important to know the dependencies between the magnitudes of the governing factors and the SI characteristics. The influence of burnishing force  $F_b$  and number of passes  $n$  on the roughness and microhardness parameters of 304 steel was established in Maximov et al. [11]. Maximov et al. [29] investigated the effects of the five main governing factors ( $r$ ,  $F_b$ ,  $f$ ,  $v$ , and  $n$ ) on the SI characteristics of 304 steel, examining one factor at a time. Skoczylas et al. [42] studied the effects of  $F_b$  and  $f$  on the surface texture of 321 steel. The effects of  $F_b$ ,  $f$ , and  $v$  on the roughness and microhardness of 304 steel were studied in Ichkova [43] and Varga and Ferencsik [44], respectively. The influence of burnishing force on the SI was investigated in Felhő and Varga [45] and Kuznetsov et al. [46]. However, there are no mathematical models (explicit relationships) relating the SI characteristics of chromium-nickel austenitic stainless steels to all five main governing factors. The availability of such a model would allow for the correct selection of the governing factor magnitudes of the DB process, so as to achieve the desired performance properties of the diamond-burnished component [47].

Thus, the aim of this study is to find explicit relationships between the five governing factors of the DB process of AISI 304 stainless steel and the most commonly used characteristics of SI, such as the average roughness parameter  $R_a$ , shape roughness skewness ( $R_{sk}$ ), kurtosis ( $R_{ku}$ ), and microhardness HV. Based on these correlations, optimizations of the DB process will be performed, depending on the functional purpose of the treated surface.

## 2. Materials and Methods

AISI 304 steel was obtained as hot-rolled bars with diameters of 16 mm and was used in the as-received state. The chemical composition was established using optical emission spectrometry. Tensile tests at room temperature were carried out using a Zwick/Roell Vibrophore 100 testing machine. The working sections of the tensile test specimens have a diameter of 6 mm and a length of 30 mm. The hardness was measured via a VEB-WPM tester using a spherical-ended indenter with a diameter of 2.5 mm, a loading of 63 kg, and a holding time of 10 s.

DB was undertaken on an Index Traub CNC lathe using conventional flood lubrication (Vasco 6000). The kinematic scheme and burnishing device are shown in Figure 1. The burnishing devices provide elastic normal contact between the deforming element and the treated surface. Turning as pre-machining and DB were carried out on the CNC lathe in one clamping process to minimize the concentric run-out in DB. A VCMT 160404 – F3P carbide cutting insert (main back angle  $\alpha_0 = 7^\circ$ ; radius at tool tip 0.4 mm) was used for the previous turning. SVJCR 2525M-16 holder with main and auxiliary setting angles  $\chi_c = 93^\circ$  and  $\chi'_c = 52^\circ$ , respectively, was used. The cutting insert and the holder are manufactured by ISCAR Bulgaria. The average roughness  $R_a$  before DR was  $Ra^{init} = 0.529 \mu m$ .

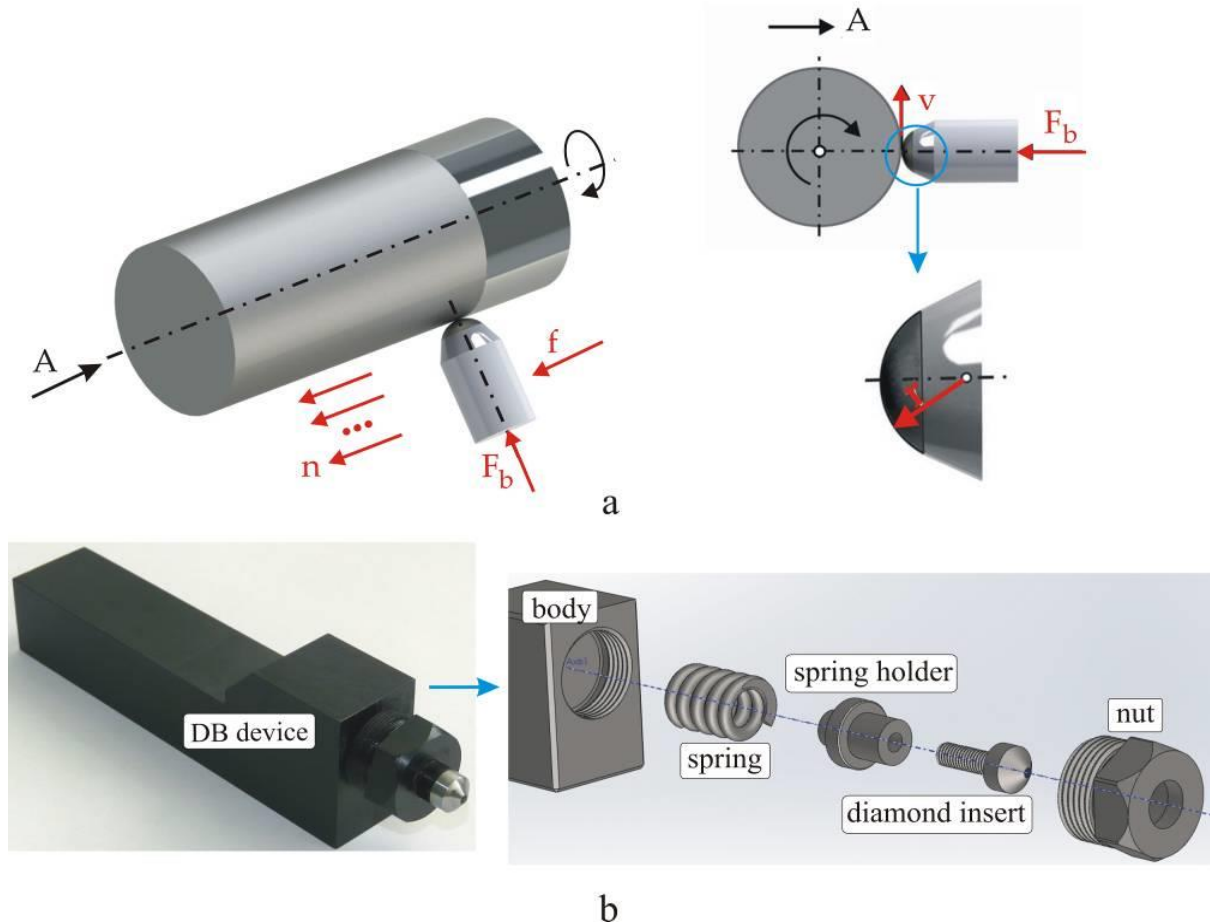


**Figure 1.** DB implementation: A. kinematics and governing factors; b. DB device.

2D roughness parameters were measured using a Mitutoyo SurfTest SJ-210 surface roughness tester with a base length of 0.8 mm. The final results were obtained as average arithmetic values from the measurements taken at six equally spaced test points.

ZHV $\mu$  Zwick/Roell microhardness tester (Ulm, Germany) was used to establish the surface microhardness. The loading and holding time were 0.05 kgf and 10 s, respectively. The final surface microhardness value was the center of clustering of ten measurements.

### 3. Results and Discussion

#### 3.1. Material Used

Table 1 shows the chemical composition of the used AISI 304 steel. The remaining chemical elements (0.203 wt%) are Ti, Al, Pb, Sn, Nb, B, As, Zn, Bi, Zr and Ca. The main mechanical characteristics of the as-received material are shown in Table 2.

**Table 1.** Chemical composition (in wt%) of the used AISI 304 stainless steel.

Fe	C	Si	Mn	P	S	Cr	Ni	Mo	Cu	Co	V	W	other
69.51	0.023	0.271	1.600	0.047	0.034	19.19	7.98	0.243	0.637	0.161	0.060	0.04	Balance

**Table 2.**

Main mechanical characteristics of the used AISI 304 steel (as-received).

Yield limit, MPa	Tensile strength, MPa	Elongation, %	Hardness, HB
338 <sup>+9</sup> <sub>-18</sub>	733 <sup>+12</sup> <sub>-10</sub>	44.7 <sup>+0.3</sup> <sub>-0.2</sub>	250 <sup>±8</sup>

3.2. Experimental Design

3.2.1. Governing Factors, Levels, And Objective Functions

The governing factors were the burnishing force  $F_b$ , the feed rate  $f$ , the burnishing velocity  $v$ , the diamond insert radius  $r$ , and the number of passes  $n$  (Figure 1a). For the experimental points where  $n > 1$ , a one-way working scheme was used. The governing factor magnitudes were selected based on the results obtained in Maximov et al. [29], one factor at a time. These results show that: 1) a burnishing force exceeding 500 N or below 100 N deteriorates the roughness  $R_a$ ; 2) a feed rate exceeding 0.08 mm/rev increases  $R_a$ ; and 3) the SI characteristics are not appreciably changed after 5 passes. In addition, according to Maximov et al. [38], high burnishing velocities (over 150 m/min) lead to a softening effect, reducing surface microhardness and residual compressive stresses. On this basis, the levels of the governing factors are defined as shown in Table 3.

**Table 3.**

Governing factors and their levels.

Governing factors	Levels							
	Natural, $\tilde{x}_i$				Coded, $x_i$			
Burnishing force $F_b$ [N]	$\tilde{x}_1$	100	300	500	$x_1$	-1	0	1
Feed rate $f$ [mm/rev]	$\tilde{x}_2$	0.02	0.05	0.08	$x_2$	-1	0	1
Burnishing velocity $v$ [m/min]	$\tilde{x}_3$	50	85	120	$x_3$	-1	0	1
Diamond insert radius $r$ [mm]	$\tilde{x}_4$	2	3	4	$x_4$	-1	0	1
Number of passes $n$	$\tilde{x}_5$	1	3	5	$x_5$	-1	0	1

The transformation from physical (natural)  $\tilde{x}_i$  to dimensionless  $x_i$  variables is performed using the formula:

$$x_i = \frac{(\tilde{x}_i - \tilde{x}_{i,0})}{(\tilde{x}_{i,max} - \tilde{x}_{i,0})}, \tag{1}$$

where  $\tilde{x}_{i,0}$  and  $\tilde{x}_{i,max}$  are the average and maximum value of the physical variable respectively.

The selected objective functions were the roughness parameters  $R_a$ ,  $R_{sk}$ ,  $R_{ku}$  and microhardness HV:  $Y_{Ra}$ ,  $Y_{sk}$ ,  $Y_{ku}$ , and  $Y_{HV}$  respectively. The reasons for choosing these SI characteristics are as follows: 1)  $R_a$  represents the surface height variation and is the most used roughness parameter in engineering practice; 2) the average roughness  $R_a$  and the shape roughness parameters (skewness and kurtosis) play significant roles in describing the operational behavior of the diamond burnished surface [11, 14-16] and 3) the surface microhardness is closely correlated with the wear and fatigue behaviour of the diamond burnished component [11].

3.2.2. Planned Experiment

A planned experiment and a second-order (the factors change at three levels and the approximating polynomial cannot be higher than second order) optimal composition design were used (Table 4). Since the number of governing factors is relatively large, the number of experimental points is expected to be,  $N = 2^5 + 5 \times 2 = 42$ . To reduce the number of experimental points within the experimental design scheme, a fractional replica was used for the design core [48]. The diamond insert radius ( $x_4$ ) and the number of passes ( $x_5$ ) accept only integer values. In this study, the coded values of these two governing factors were assumed to be equal to the higher interactions between the first three factors ( $x_i, i = 1, 2, 3$ ) as follows:  $x_4 = x_1x_2x_3$  and  $x_5 = -x_2x_3$ . Thus, while preserving the properties of the original design, the number of experimental points is reduced to 18 ( $N = 2^3 + 5 \times 2 = 18$ ). It is important to note that the fractional replica does not allow to separation of the influence of  $x_4$  (respectively of  $x_5$ ) from the influence of the interaction  $x_1x_2x_3$  (respectively of  $x_2x_3$ ).

**Table 4.**

Experimental design, experimental results, and predicted values.

No.	$F_b$		$f$	$v$	$r$	$n$	Ra, $\mu\text{m}$		Rsk		Rku		HV0.05	
	$x_1$	$x_2$	$x_3$	$x_4$	$x_5$	Exp.	$Y_{Ra}$	Exp.	$Y_{sk}$	Exp.	$Y_{Rku}$	Exp.	$Y_{HV}$	
1	-1	-1	-1	-1	-1	0.127	0.1265	0.187	0.1870	2.590	2.5344	579	579.05	
2	1	-1	-1	1	-1	0.138	0.1375	0.139	0.1390	2.865	2.9322	484	484.05	
3	-1	1	-1	1	1	0.067	0.0665	-0.930	-0.9300	4.766	4.7104	440	440.05	
4	1	1	-1	-1	1	0.198	0.1975	0.353	0.3530	3.078	3.1452	658	658.05	
5	-1	-1	1	1	1	0.133	0.1325	-0.023	-0.0230	3.468	3.5352	432	432.05	
6	1	-1	1	-1	1	0.129	0.1300	0.102	0.1020	3.223	3.1674	631	631.05	
7	-1	1	1	-1	-1	0.133	0.1325	0.590	0.5900	3.395	3.4622	492	492.05	
8	1	1	1	1	-1	0.132	0.1315	0.061	0.0610	2.718	2.6624	462	462.05	
9	-1	0	0	0	0	0.066	0.0663	-0.301	-0.3010	4.128	4.1048	437	436.79	
10	1	0	0	0	0	0.092	0.0923	0.042	0.0420	2.873	2.8498	489	488.79	
11	0	-1	0	0	0	0.060	0.0673	0.090	0.1040	3.434	3.5037	470	469.79	
12	0	1	0	0	0	0.074	0.0673	0.118	0.1040	2.825	2.8947	443	442.79	
13	0	0	-1	0	0	0.066	0.0643	0.040	0.0400	2.627	2.6038	462	460.79	
14	0	0	1	0	0	0.062	0.0643	0.148	0.1480	2.889	2.8658	460	460.79	
15	0	0	0	-1	0	0.112	0.1083	-0.647	-0.6470	4.852	4.8288	634	633.79	
16	0	0	0	1	0	0.104	0.1083	0.067	0.0670	2.762	2.7388	469	468.79	
17	0	0	0	0	-1	0.070	0.0625	-0.010	-0.0165	2.935	2.8703	473	473.62	
18	0	0	0	0	1	0.057	0.0625	-0.023	-0.0165	2.852	2.8703	465	465.62	

3.3. Experimental Results and Models

The obtained experimental results are shown in Table 4. Regression analyses were performed using QStatLab software [50]. Given the chosen experimental design, the approximating polynomials are of at most second order:

$$Y^{(k)}(\{X\}) = b_0^{(k)} + \sum_{i=1}^3 b_i^{(k)} x_i + \sum_{i=1}^2 \sum_{j=i-1}^3 b_{ij}^{(k)} x_i x_j + \sum_{i=1}^3 b_{ii}^{(k)} x_i^2, \quad k = 1, 2, 3, 4, \tag{2}$$

where  $\{X\}$  is the vector of the governing factors  $x_i$ , and  $k = 1, 2, 3$  shows the corresponding objective function:  $Y_{Ra}$ ,  $Y_{sk}$ ,  $Y_{ku}$ , and  $Y_{HV}$ , respectively.

The polynomial coefficients of the four objective functions are shown in Table 5. The threshold for statistical significance is  $p = 0.05$ . Table 4 shows the values predicted by the models at the experimental points; they agree well with the experiment.

**Table 5.**  
Regression coefficients.

$b_{ij}$	$Y_{Ra}$	$Y_{sk}$	$Y_{ku}$	$Y_{HV}$
$b_0$	0.06245283	-0.07446875	3.19915090	469.62264000
$b_1$	0.01300000	0.17150000	-0.62750000	26.00000000
$b_2$	N	N	-0.30450000	-13.50000000
$b_3$	N	0.05400000	0.13100000	N
$b_4$	N	0.35700000	-1.04500000	-82.50000000
$b_5$	N	N	N	-4.00000000
$b_{11}$	0.01689623	-0.05503125	0.27813208	-6.83018870
$b_{22}$	0.00489623	0.17846875	N	-13.33018900
$b_{33}$	0.00189623	0.16846875	-0.46436792	-8.83018870
$b_{44}$	0.04589623	-0.21553125	0.58463208	81.66981100
$b_{55}$	N	0.05796875	-0.32886792	N
$b_{12}$	0.01537500	0.08462500	-0.29937500	10.50000000
$b_{13}$	N	-0.20487500	N	5.75000000
$b_{14}$	N	0	0	N
$b_{15}$	0.01462500	0.60512500	-1.23637500	-14.75000000
$b_{23}$	N	0.18437500	-0.37087500	-22.00000000
$b_{24}$	-0.01837500	0	0	N
$b_{25}$	N	-0.06862500	0.19287500	18.00000000
$b_{34}$	N	0	0	N
$b_{35}$	N	0.04137500	-0.53087500	-4.25000000
$b_{45}$	-0.00412500	0.06762500	-0.33562500	-10.50000000

N – the coefficient is ignored as a very small quantity

The critical values of the Student ( $t$ ) and Fisher ( $F$ ) statistics, residual standard deviation (ResStDev), correlation coefficient ( $R^2$ ), and adjusted correlation coefficient ( $R_{adj}^2$ ) [49] for the four models are shown in Table 6. The results confirm the adequacy of the models.

**Table 6.**  
Results from the statistical analysis of the regression models.

Model	$T$	$F$	Res St. Dev	$R^2$	$Radj^2$
$Y_{Ra}$	2.30600	3.38813	0.0053514	0.99115	0.9812
$Y_{Sk}$	4.30265	19.42914	0.015435	0.99976	0.99794
$Y_{ku}$	3.18245	8.71490	0.12631	0.99399	0.96597
$Y_{HV}$	4.30265	19.42914	1.2533	0.99997	0.9997

The dimensionless absolute values of the coefficients  $b_i$  and  $b_{ij}$  indicate the significance of the corresponding governing factor. The larger the absolute value, the stronger the influence of the respective governing factor. The burnishing force and the diamond insert radius exert the strongest influences on the average roughness  $R_a$ . The skewness is most strongly influenced by the diamond insert radius, followed by the feed rate and burnishing force. However, the coefficient  $b_{15}$  for interaction between burnishing force and number of passes exhibits the largest magnitude. So, based only on the magnitudes of the coefficients, the influences on skewness cannot be graded. The kurtosis is most strongly influenced by diamond insert radius and burnishing force, while burnishing velocity exerts the least influence. However, in this case too, the coefficient  $b_{15}$  for interaction between burnishing force and number of passes has the largest magnitude. The radius of the diamond insert exerts the strongest influence on the surface microhardness, followed by the burnishing force. It should be noted that the coefficients  $b_4$  and  $b_5$  give a mixed estimate, i.e., they estimate the simultaneous influence of  $x_4$  and of the interaction  $x_1x_2x_3$  (the simultaneous influence of  $x_5$  and of the interaction  $x_2x_3$ , respectively).

The dimensionless absolute values of the coefficients  $b_{ij}, i \neq j$ , give an information for the interaction  $x_i x_j, i \neq j$ , between the corresponding factors. The strongest influence on the average roughness  $R_a$  is exerted by the interaction between the feed rate and the diamond insert radius, i.e.,  $x_2x_4$ , indicated by the coefficient  $b_{24}$  have largest magnitude in the  $R_a$  model. The explanation is that the theoretical (kinematic) roughness  $R_a$  depends precisely on these two governing factors:

$Ra \approx \frac{f^2}{31.2r}$  [27]. The interaction between the feed rate and burnishing velocity has the greatest influence on the microhardness ( $b_{23}$  has the largest absolute value in the HV model). The feed rate directly influences the cyclic loading

coefficient [50], which measures strain hardening. The burnishing velocity directly affects the amount of heat generated from both friction and surface plastic deformation, which causes softening [51]. The interaction between these two governing factors indicates which of the two effects (mechanical due to strain hardening or thermal due to the generated heat) predominates for the specific combination of factor magnitudes. It is very difficult to provide a physical interpretation of the effects of interactions between the factors on the shape roughness parameters (skewness and kurtosis).

Comparing dimensionless coefficients provides an approximate idea of the influence of the governing factors on the respective objective function. Therefore, an analysis of variance (ANOVA) was performed. The results (main effects) are shown in Figures 2 to 5.

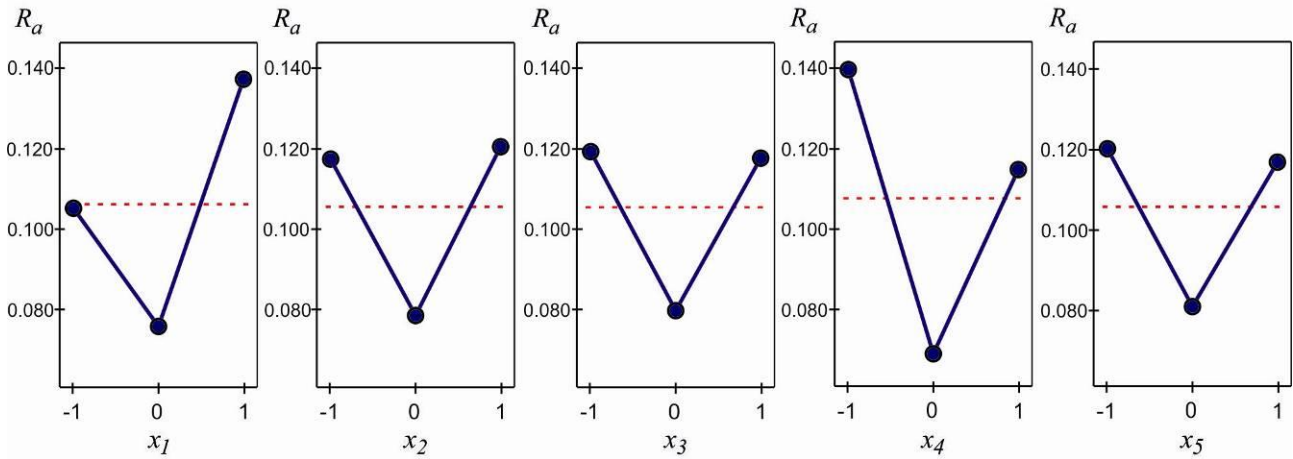


**Figure 2.** ANOVA main effects for the average roughness  $R_a$ .

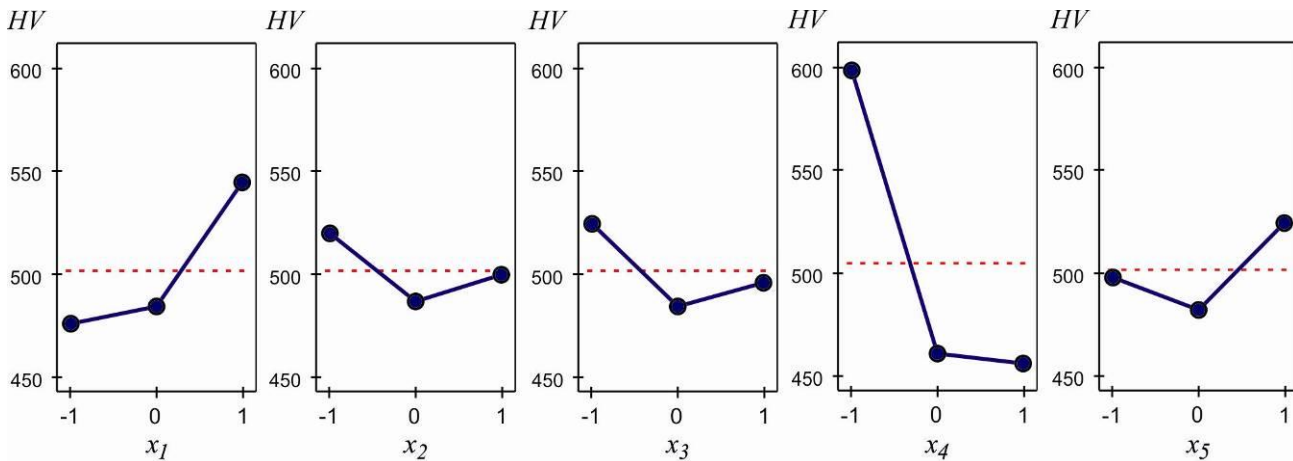


**Figure 3.** ANOVA main effects for the surface microhardness HV.

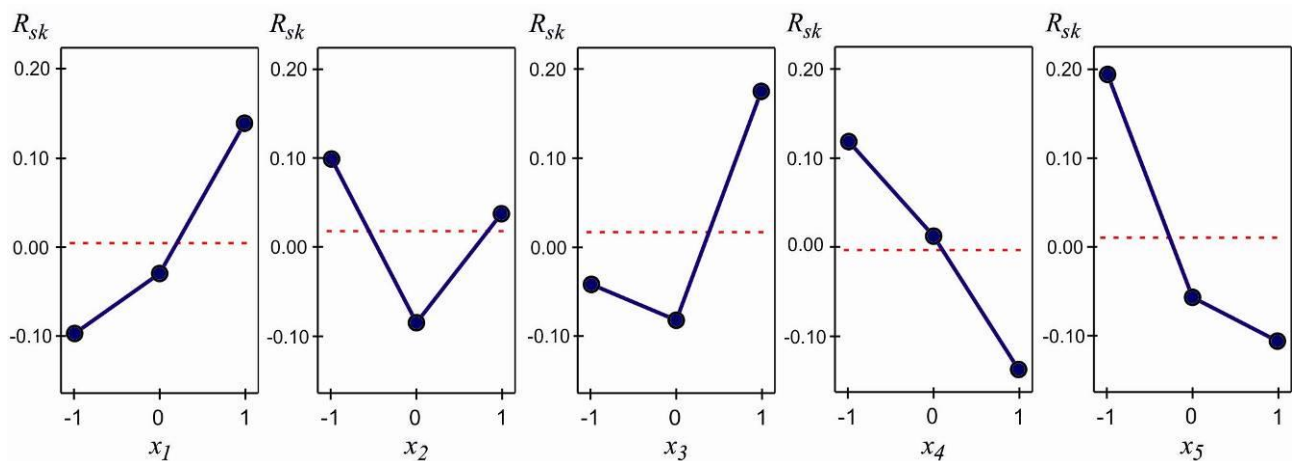


**Figure 4.** ANOVA main effects for the skewness  $R_{sk}$ .

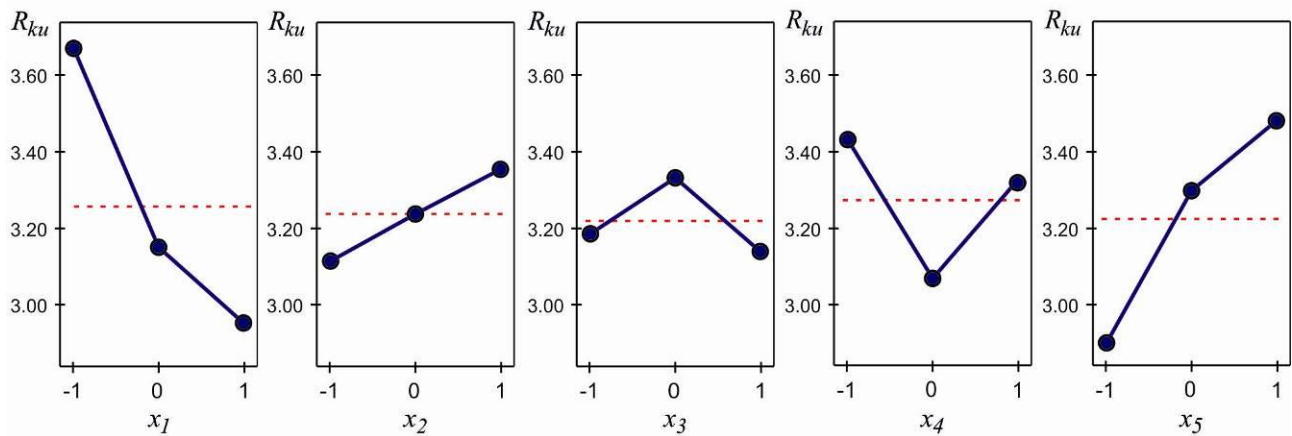


**Figure 5.**  
ANOVA main effects for the kurtosis  $R_{ku}$ .

The ANOVA outcomes confirm and complement the conclusions drawn about the significance of the governing factors in the objective functions. The diamond insert radius has the strongest influence on the average roughness  $R_a$ , followed by the burnishing force and feed rate. The influence of the other two factors is practically equivalent and the least significant. In principle, achieving a minimum average roughness  $R_a$  is important for improving fatigue behavior [12]. The smallest value of  $R_a$  is obtained when the five governing factors are maintained at average levels (Figure 2). The strongest influence on the surface microhardness is exerted by diamond radius, followed by burnishing force. The influence of the other factors is weaker and practically equivalent. The highest microhardness is achieved when burnishing force and number of passes are maintained at upper levels, and the other three factors at lower levels (Figure 3). The strongest influence on the skewness is exerted by the number of passes, followed by the burnishing velocity and the diamond radius, which have equal weight. The weakest influence is the feed rate. Negative skewness occurs when the burnishing force and burnishing velocity are maintained at medium or low levels, the feed rate is medium, the radius is largest, and the number of passes is maintained at medium or high levels (Figure 4). As is known [13-15, 52], negative skewness favors the tribological behavior of the surface under boundary lubrication conditions, due to the deep valleys that retain oil. At the same time, negative skewness worsens the fatigue behavior because the deep valleys are natural stress concentrators [11]. Conversely, positive skewness improves the fatigue behavior of the surface. The combination of high levels of burnishing force and burnishing velocity, low or high levels of the feed rate, and low or medium levels of the diamond radius of single-pass DB leads to positive skewness (Figure 4). The strongest influence on the kurtosis is exerted by the burnishing force, followed by the number of passes and diamond radius. The weakest (and practically equivalent) influence is exerted by the feed rate and burnishing velocity. It is known that the maximum kurtosis (greater than 3) favors both wear resistance in the condition of boundary lubrication [14, 15] and fatigue strength (when the finishing is DB) [11]. The maximum absolute kurtosis is obtained when the burnishing force occupies a lower level, the feed rate is maximum, the burnishing velocity occupies a middle level, the diamond radius is minimal, and a number of passes occupies an upper level (Figure 5). It should be borne in mind that ANOVA results are based only on the results at the experimental points.

Graphical visualizations of the four models are shown in Figures 6 to 9. Visual inspection of the surfaces confirms the conclusions drawn about the significance of the governing factors and shows that the extreme values of the objective functions may be at points on the hypersurfaces that do not coincide with the points of the experimental design.

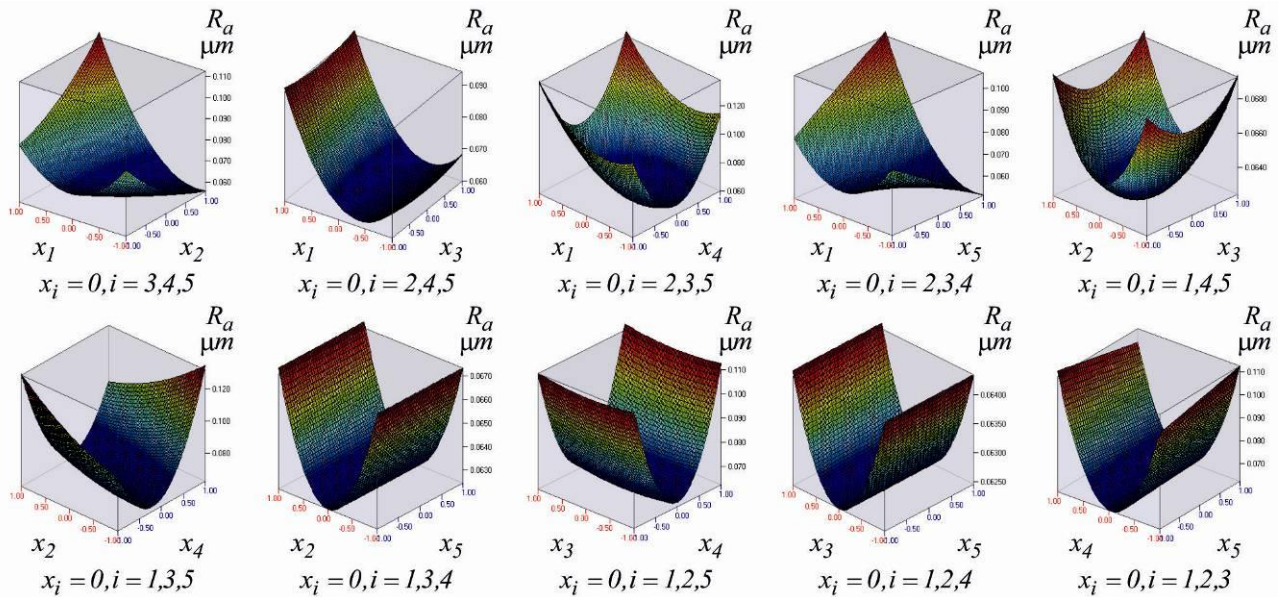


**Figure 6.**  
Graphical visualization of the average roughness model.

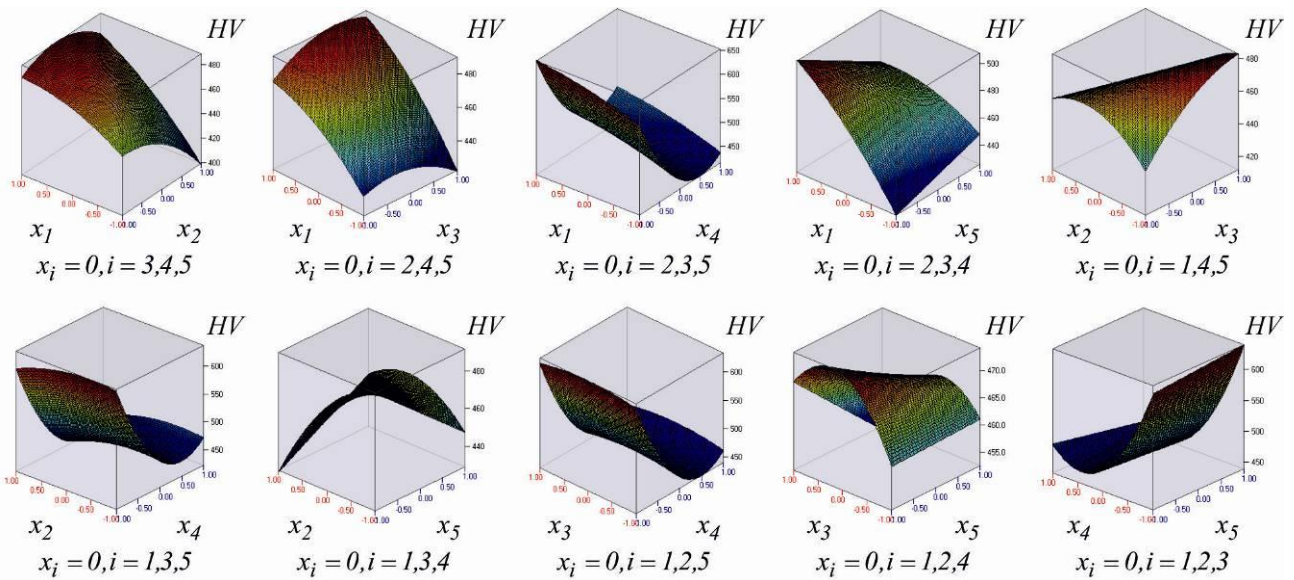


**Figure 7.**  
Graphical visualization of the surface microhardness model.

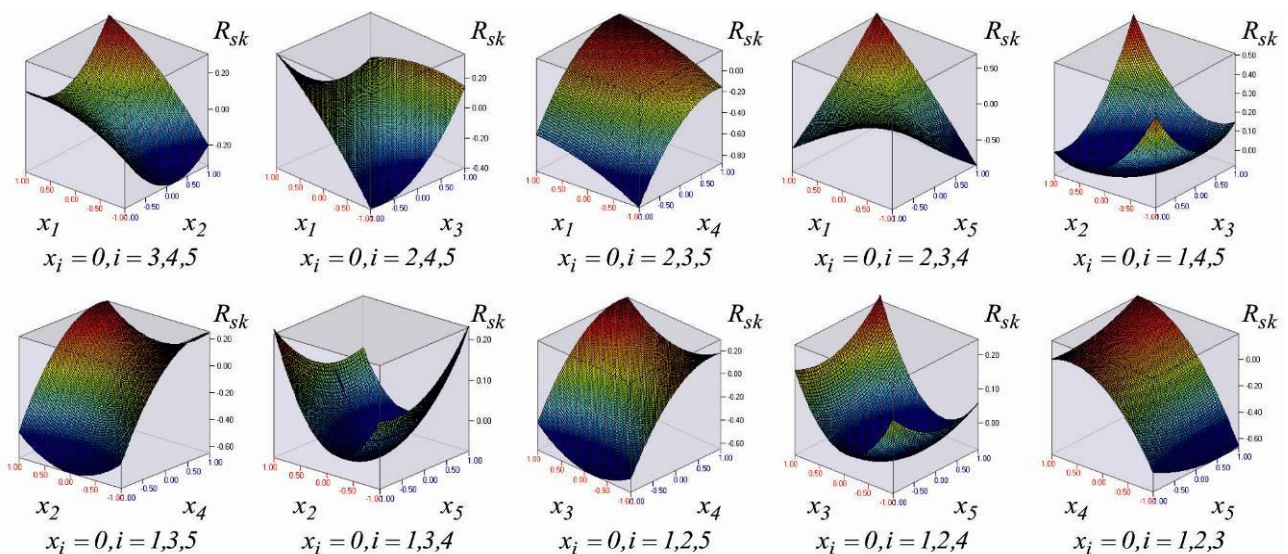


**Figure 8.**  
Graphical visualization of the skewness model.

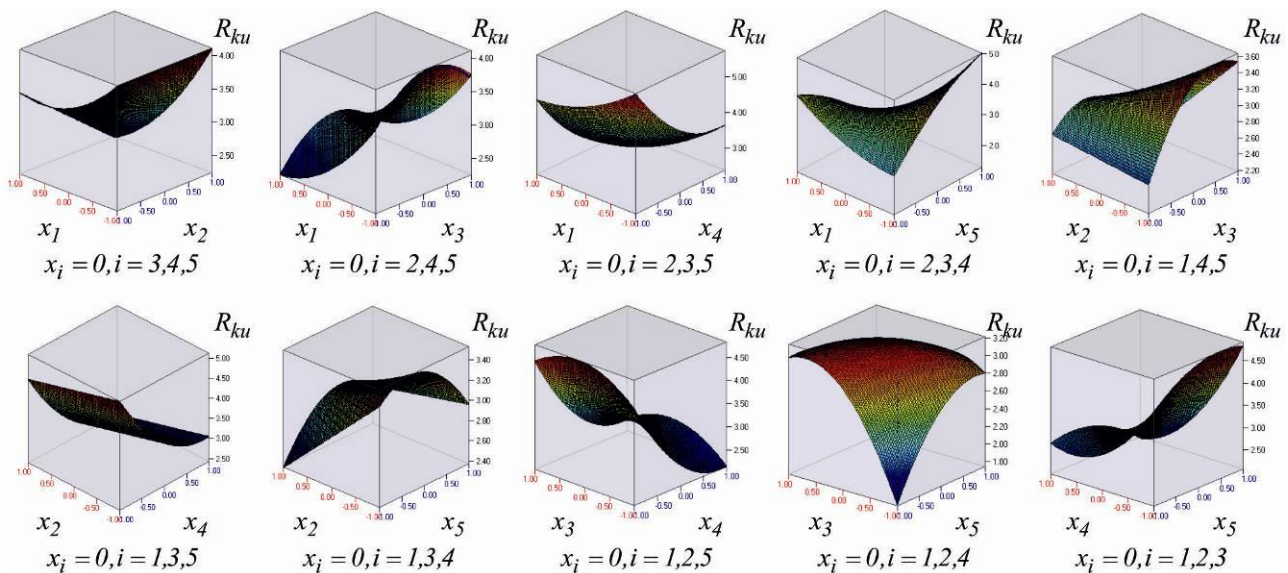


**Figure 9.**  
Graphical visualization of the kurtosis model.

### 3.4. Optimizations

It is known Maximov et al. [33] and Korzynski [53] that DB can be implemented as a smoothing or hardening process, or a mixture of both. The main purpose of smoothing is to achieve the lowest possible roughness of the burnished surface. The remaining beneficial effects (increased microhardness and compressive residual stresses) also occur, but are less pronounced than when hardening. Hardening DB aims primarily to maximize the strain hardening effect. Similar to Ecorol's deep rolling process [54], hardening DB aims to simultaneously achieve three effects: smoothing, significant cold work, and the introduction of significant residual compressive stresses. While optimizing either smoothing or hardening alone is a single-objective task, mixed DB requires multi-objective optimizations depending on the functional purpose of the diamond-burnished component.

It should be borne in mind that the optimal values of diamond radius ( $x_4^*$  and  $r^*$ , respectively) and number of passes ( $x_5^*$  and  $n^*$ , respectively) can only be integers.

#### 3.4.1. One-Objective Optimizations

To find the minimum of the roughness parameter  $R_a$  and the values of governing factors (integer values for diamond radius and number of passes) that provide it, the minimum of the objective function  $Y_{Ra}$  was found using QStatLab and the SCAN method [49]. The optimal values of the driving factors are the average levels of all factors ( $x_i^* = 0, i = 1, 2, 3, 4, 5$ ). The minimum value of the average roughness  $R_a$  with the imposed constraint for integer values of the radius and number of passes is  $\min R_a = 0.0624 \mu m$ , and the remaining objective functions take the following values:  $Y_{sk} = -0.074$ ,  $Y_{ku} = 3.199$ ,  $Y_{HV} = 469.62$ . Based on the results obtained in Korzynski et al. [13], Sedlaček et al. [14], Duncheva et al. [15] and Duncheva et al. [52] it can be expected that this combination of SI characteristics (mirror-like surface, negative skewness and kurtosis greater than three) increases wear resistance under the boundary lubrication condition.

The maximum surface microhardness was obtained using the same method in QStatLab. The optimal values of the control factors are as follows:  $x_1^* = 1$ ,  $x_2^* = -1$ ,  $x_3^* = 1$ ,  $x_4^* = -1$ , and  $x_5^* = -1$ . The maximum microhardness is  $\max HV = 692.1$ , and the remaining objective functions take the following values:  $Y_{Ra} = 0.0925 \mu m$ ,  $Y_{sk} = -1.19$ , and  $Y_{ku} = 6.41$ . The resulting combination of low average roughness  $R_a$ , more negative skewness, and kurtosis significantly greater than three is particularly suitable when the requirement is for high wear resistance under boundary lubrication conditions. However, given the significant negative skewness, this combination is not suitable for maximizing fatigue strength due to the significant stress concentrators [11].

The highest microhardness established by ANOVA is the value at the fourth experimental point of the experimental design (see Table 4),  $HV = 658$ , while the optimal values of the governing factors and the maximum microhardness correspond to a point in the factor space that does not coincide with a vertex or the middle of a wall of the hypercubic space.

#### 3.4.2. Multi-objective optimization

Taguchi's methods and ANOVA are not suitable for multi-objective optimization. In this study, QStatLab, which implements the non-dominated sorting genetic algorithm NSGA II, was used [49, 55].

It is known that small values of the roughness parameter  $R_a$  favor fatigue strength [12] as they reduce the surface stress concentrators. Conversely, more negative skewness negatively affects fatigue strength, due to the deep valleys naturally

concentrating stress [11]. According to Zabala et al. [16], kurtosis greater than three worsens the fatigue behavior. This statement has a sound physical basis considering the sharp peaks and deep valleys of a kurtotic surface profile. However, surface texture is not an independent factor when formed by DB, since the severe surface plastic deformation, characteristic of DB, introduces such beneficial effects as high surface microhardness, residual compressive stresses and grain refinement. For example, in Maximov et al. [11], it was experimentally proven that, with increasing kurtosis, the rotating bending fatigue limit of diamond-burnished AISI 304 steel specimens increases. The explanation in Maximov et al. [11] is that, with increasing burnishing force and number of passes, the kurtosis increases; however, at the same time, the microhardness and the depth of the residual compressive stress zone both increase. The latter two positive effects neutralize the isolated negative effect of kurtosis and increase the fatigue strength. Thus, high values of kurtosis on the DBed surface are indicators of significant introduced residual compressive stresses and significant surface microhardness.

To find the values of the governing factors that increase the rotating bending fatigue limit of the diamond burnished AISI 304 steel specimens, the following multi-objective optimization task is set. The vector of the objective functions  $\{Y(\{X\})\} = [Y_{Ra} \ Y_{HV}]^T$  is known. The optimal sizes  $x_i^*, i = 1, 2$  of the governing factors must be found, for which  $Y_{Ra}(\{X\}^*) \rightarrow \min$ ,  $Y_{HV}(\{X\}^*) \rightarrow \max$  and the skewness is positive. The following functional constraints were imposed:  $Y_{Ra} < 0.12 \mu m$ ,  $Y_{HV} > 600$ , and  $Y_{Rsk} > 0$ . A Pareto optimal solution approach, QStatLab and NSGA II were used. The resulting Pareto front is shown in Figure 10. The selected compromise for an optimal solution provides integer values of diamond radius and number of passes (Table 7).

**Table 7.**  
Compromise optimal values of the governing factors and objective functions.

Compromise optimal values of the governing factors					Compromise optimal values of the objective functions			
Coded (Dimensionless)					$Y_{Ra}, \mu m$	$Y_{HV}$	$Y_{Rsk}$	$Y_{Rku}$
$x_1^*$	$x_2^*$	$x_3^*$	$x_4^*$	$x_5^*$				
0.6616	-0.7937	-0.8262	-1	0.5097	0.1131	614.06	0.0086	4.08
Natural (physical)								
$F_b^*, N$	$f^*, mm/rev$	$v^*, m/min$	$r^*, mm$	$n^*$				
432	0.0262	56	2	4				

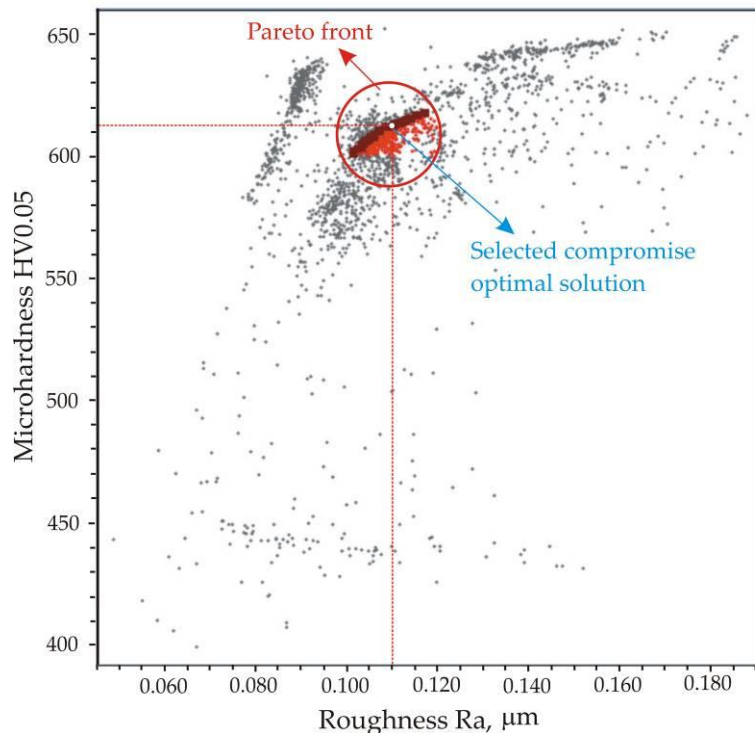


**Figure 10.**  
Pareto front and selected compromise optimal solution.

#### 4. Conclusions

The purpose of this research was to find explicit correlations between the five main governing factors of the DB process of 304 stainless steel and the most frequently used SI characteristics, such as the average roughness parameter  $R_a$ , shape roughness parameters skewness ( $R_{sk}$ ) and kurtosis ( $R_{ku}$ ), and microhardness HV. A planned experiment with a second-order

composition plan, analysis of variance (ANOVA), regression analyses, and woptimizations were employed to achieve the goal.

As a result of this work, the major new findings concerning the nature of DB were:

- Explicit relationships between all governing factors of the database and the main surface integrity characteristics (average roughness  $R_a$ , skewness, kurtosis, and microhardness) were established.
- The significance of the governing factors for the individual characteristics of SI was found.
- The optimal values of the governing factors were found through single- and multi-objective optimizations, depending on the functional purpose of the diamond-burnished surface.

## References

- [1] Grand View Research Company, *Stainless steel market size, share & trends analysis report by grade (300 Series, Duplex Series), by product (Flat, Long), by application (Building & Construction, Consumer Goods), by region, and segment forecast, 2024–2030 (Report ID: 978-1-68038-945-6)*. USA: Grand View Research Company, 2024.
- [2] J. Kaleycheva, *Material science*. Sofia, Bulgaria: Scientific and Technical Union of Mechanical Engineering "Industria 4.0", 2018.
- [3] A. Hedayati, A. Najafizadeh, A. Kermanpur, and F. Forouzan, "The effect of cold rolling regime on microstructure and mechanical properties of AISI 304L stainless steel," *Journal of Materials Processing Technology*, vol. 210, no. 8, pp. 1017-1022, 2010. <https://doi.org/10.1016/j.jmatprotec.2010.02.010>
- [4] B. R. Kumar, A. Singh, S. Das, and D. Bhattacharya, "Cold rolling texture in AISI 304 stainless steel," *Materials Science and Engineering: A*, vol. 364, no. 1-2, pp. 132-139, 2004. <https://doi.org/10.1016/j.msea.2003.08.012>
- [5] F. Borgioli, "From austenitic stainless steel to expanded austenite-S phase: Formation, characteristics and properties of an elusive metastable phase," *Metals*, vol. 10, no. 2, p. 187, 2020. <https://doi.org/10.3390/met10020187>
- [6] Y. Hoshiyama, R. Mizobata, and H. Miyake, "Mechanical properties of austenitic stainless steel treated by active screen plasma nitriding," *Surface and Coatings Technology*, vol. 307, pp. 1041-1044, 2016. <https://doi.org/10.1016/j.surfcoat.2016.07.032>
- [7] I. Nikitin and I. Altenberger, "Comparison of the fatigue behavior and residual stress stability of laser-shock peened and deep rolled austenitic stainless steel AISI 304 in the temperature range 25–600 C," *Materials Science and Engineering: A*, vol. 465, no. 1-2, pp. 176-182, 2007. <https://doi.org/10.1016/j.msea.2007.02.004>
- [8] P. Juijerm and I. Altenberger, "Fatigue performance enhancement of steels using mechanical surface treatments," *Journal of Metals, Materials and Minerals*, vol. 17, no. 1, pp. 59–65, 2007.
- [9] Y. Lin, J. Lu, L. Wang, T. Xu, and Q. Xue, "Surface nanocrystallization by surface mechanical attrition treatment and its effect on structure and properties of plasma nitrided AISI 321 stainless steel," *Acta Materialia*, vol. 54, no. 20, pp. 5599-5605, 2006. <https://doi.org/10.1016/j.actamat.2006.08.014>
- [10] J. Maximov, G. Duncheva, A. Anchev, V. Dunchev, and Y. Argirov, "Improvement in fatigue strength of chromium–nickel austenitic stainless steels via diamond burnishing and subsequent low-temperature gas nitriding," *Applied Sciences*, vol. 14, no. 3, p. 1020, 2024. <http://dx.doi.org/10.3390/app14031020>
- [11] J. T. Maximov, G. V. Duncheva, A. P. Anchev, and V. P. Dunchev, "Explicit correlation between surface integrity and fatigue limit of surface cold worked chromium-nickel austenitic stainless steels," *The International Journal of Advanced Manufacturing Technology*, vol. 133, no. 11, pp. 6041-6058, 2024. <http://dx.doi.org/10.1007/s00170-024-14113-6>
- [12] P. Pawlus, R. Reizer, and M. Wieczorowski, "Functional importance of surface texture parameters," *Materials*, vol. 14, no. 18, p. 5326, 2021. <https://doi.org/10.3390/ma14185326>
- [13] M. Korzynski, K. Dudek, B. Kruczek, and P. Kocurek, "Equilibrium surface texture of valve stems and burnishing method to obtain it," *Tribology International*, vol. 124, pp. 195-199, 2018. <https://doi.org/10.1016/j.triboint.2018.04.014>
- [14] M. Sedlaček, B. Podgornik, and J. Vižintin, "Correlation between standard roughness parameters skewness and kurtosis and tribological behaviour of contact surfaces," *Tribology International*, vol. 48, pp. 102-112, 2012. <https://doi.org/10.1016/j.triboint.2011.11.008>
- [15] G. Duncheva, J. Maximov, A. Anchev, V. Dunchev, Y. Argirov, and M. Kandeveva-Ivanova, "Enhancement of the wear resistance of CuAl9Fe4 sliding bearing bushings via diamond burnishing," *Wear*, vol. 510, p. 204491, 2022. <https://doi.org/10.1016/j.wear.2022.204491>
- [16] A. Zabala, L. Blunt, W. Tato, A. Aginagalde, X. Gomez, and I. Llavori, "The use of areal surface topography characterisation in relation to fatigue performance," *MATEC Web of Conferences*, vol. 165, p. 14013, 2018. <http://dx.doi.org/10.1051/mateconf/201816514013>
- [17] Y. Luo *et al.*, "Effect of ultrasonic rolled material layer on the corrosion fatigue resistance of railway axle EA4T alloy steel," *Engineering Failure Analysis*, vol. 157, p. 107895, 2024. <https://doi.org/10.1016/j.engfailanal.2023.107895>
- [18] K. Konefal, M. Korzynski, Z. Byczkowska, and K. Korzynska, "Improved corrosion resistance of stainless steel X6CrNiMoTi17-12-2 by slide diamond burnishing," *Journal of Materials Processing Technology*, vol. 213, no. 11, pp. 1997-2004, 2013. <https://doi.org/10.1016/j.jmatprotec.2013.05.021>
- [19] G. Duncheva and J. Maximov, "Cold working technologies for increasing the fatigue life of metal structural components with fastener holes—review and perspectives," *The International Journal of Advanced Manufacturing Technology*, pp. 1-35, 2025. <https://doi.org/10.1007/s00170-025-15020-0>
- [20] G. Leghorn, "The story of shot peening," *Journal of the American Society for Naval Engineers*, vol. 69, no. 4, pp. 653-666, 1957.
- [21] K. Dai and L. Shaw, "Comparison between shot peening and surface nanocrystallization and hardening processes," *Materials Science and Engineering: A*, vol. 463, no. 1-2, pp. 46-53, 2007. <https://doi.org/10.1016/j.msea.2006.07.159>
- [22] J. Maximov, G. Duncheva, A. Anchev, V. Dunchev, Y. Argirov, and M. Nikolova, "Effects of heat treatment and diamond burnishing on fatigue behaviour and corrosion resistance of AISI 304 austenitic stainless steel," *Applied Sciences*, vol. 13, no. 4, p. 2570, 2023. <https://doi.org/10.3390/app13042570>
- [23] M. Korzynski, *Slide diamond burnishing. in: Nonconventional Finishing Technologies*, Ed. M. Korzynski. Warsaw: Polish Scientific Publishers PWN, 2013.

- [24] H. Roohi, H. Baseri, and M. J. Mirnia, "Evaluation of optimized surface characteristics in non-rotational sliding ball burnishing," *Materials and Manufacturing Processes*, vol. 39, no. 16, pp. 2299-2308, 2024. <https://doi.org/10.1080/10426914.2024.2395010>
- [25] J. Maximov, T. Kuzmanov, G. Duncheva, and N. Ganey, "Spherical motion burnishing implemented on lathes," *International Journal of Machine Tools and Manufacture*, vol. 49, no. 11, pp. 824-831, 2009. <https://doi.org/10.1016/j.ijmachtools.2009.05.011>
- [26] J. Maximov and G. Duncheva, "Finite element analysis and optimization of spherical motion burnishing of low-alloy steel," *Proceedings of the Institution of Mechanical Engineers, Part C: Journal of Mechanical Engineering Science*, vol. 226, no. 1, pp. 161-176, 2012. <https://doi.org/10.1177/0954406211412024>
- [27] A. Nestler and A. Schubert, "Effect of machining parameters on surface properties in slide diamond burnishing of aluminium matrix composites," *Materials Today: Proceedings*, vol. 2, pp. S156-S161, 2015. <https://doi.org/10.1016/j.matpr.2015.05.033>
- [28] D. Toboła *et al.*, "Microstructural dependence of tribological properties of Ti-6Al-4V ELI alloy after slide burnishing/shot peening and low-temperature gas nitriding," *Surface and Coatings Technology*, vol. 501, p. 131941, 2025. <https://doi.org/10.1016/j.surfcoat.2025.131941>
- [29] J. Maximov, G. Duncheva, A. Anchev, V. Dunchev, and Y. Argirov, "Effect of diamond burnishing on fatigue behaviour of AISI 304 chromium-nickel austenitic stainless steel," *Materials*, vol. 15, no. 14, p. 4768, 2022. <https://doi.org/10.3390/ma15144768>
- [30] E. H. Hull and A. J. Nerad, *U.S. Patent No. 2,966,722*. Washington, DC: U.S. Patent and Trademark Office, 1961.
- [31] G. Duncheva, J. Maximov, V. Dunchev, A. Anchev, T. Atanasov, and J. Capek, "Single toroidal roller burnishing of 2024-T3 Al alloy implemented as mixed burnishing process," *The International Journal of Advanced Manufacturing Technology*, vol. 111, pp. 3559-3570, 2020. <https://doi.org/10.1007/s00170-020-06350-2>
- [32] J. Maximov, G. Duncheva, A. Anchev, and V. Dunchev, "Slide burnishing versus deep rolling—A comparative analysis," *The International Journal of Advanced Manufacturing Technology*, vol. 110, pp. 1923-1939, 2020. <https://link.springer.com/article/10.1007/s00170-020-05950-2>
- [33] J. Maximov, G. Duncheva, A. Anchev, and V. Dunchev, "Smoothing, deep, or mixed diamond burnishing of low-alloy steel components—optimization procedures," *The International Journal of Advanced Manufacturing Technology*, vol. 106, pp. 1917-1929, 2020. <https://link.springer.com/article/10.1007%2Fs00170-019-04747-2>
- [34] D. Toboła and B. Kania, "Phase composition and stress state in the surface layers of burnished and gas nitrided Sverker 21 and Vanadis 6 tool steels," *Surface and Coatings Technology*, vol. 353, pp. 105-115, 2018. <https://doi.org/10.1016/j.surfcoat.2018.08.055>
- [35] Y. Argirov, J. Maximov, G. Duncheva, A. Anchev, V. Dunchev, and T. Mechkarova, "Evolution of surface integrity characteristics and mechanical behavior of diamond burnished and turned AISI 304 steel specimens after prolonged exposure to natural seawater," *Coatings*, vol. 15, no. 1, p. 31, 2025. <https://doi.org/10.3390/coatings15010031>
- [36] M. Korzynski, K. Dudek, A. Palczak, B. Kruczek, and P. Kocurek, "Experimental models and correlations between surface parameters after slide diamond burnishing," *Measurement Science Review*, vol. 18, no. 3, pp. 123-129, 2018.
- [37] D. Toboła, J. Morgiel, and L. Maj, "TEM analysis of surface layer of Ti-6Al-4V ELI alloy after slide burnishing and low-temperature gas nitriding," *Applied Surface Science*, vol. 515, p. 145942, 2020. <https://doi.org/10.1515/msr-2018-0018>
- [38] J. Maximov, G. Duncheva, A. Anchev, N. Ganey, I. Amudjev, and V. Dunchev, "Effect of slide burnishing method on the surface integrity of AISI 316Ti chromium–nickel steel," *Journal of the Brazilian Society of Mechanical Sciences and Engineering*, vol. 40, pp. 1-14, 2018. <https://doi.org/10.1007/s40430-018-1135-3>
- [39] J. T. Maximov, A. P. Anchev, G. V. Duncheva, N. Ganey, K. F. Selimov, and V. P. Dunchev, "Impact of slide diamond burnishing additional parameters on fatigue behaviour of 2024-T3 Al alloy," *Fatigue & Fracture of Engineering Materials & Structures*, vol. 42, no. 1, pp. 363-373, 2019. <https://doi.org/10.1111/ffe.12915>
- [40] G. V. Duncheva, J. T. Maximov, A. P. Anchev, V. P. Dunchev, and Y. B. Argirov, "Multi-objective optimization of the internal diamond burnishing process," *Materials and Manufacturing Processes*, vol. 37, no. 4, pp. 428-436, 2022. <https://doi.org/10.1080/10426914.2021.1981937>
- [41] M. Korzynski, K. Dudek, and K. Korzynska, "Effect of slide diamond burnishing on the surface layer of valve stems and the durability of the stem-graphite seal friction pair," *Applied Sciences*, vol. 13, no. 11, p. 6392, 2023. <http://dx.doi.org/10.3390/app13116392>
- [42] A. Skoczylas, K. Zaleski, J. Matuszak, K. Ciecieląg, R. Zaleski, and M. Gorgol, "Influence of slide burnishing parameters on the surface layer properties of stainless steel and mean positron lifetime," *Materials*, vol. 15, no. 22, p. 8131, 2022. <http://dx.doi.org/10.3390/ma15228131>
- [43] M. Ichkova, "Effects of diamond burnishing process parameters on the surface roughness of AISI 304 austenitic stainless steel," *Edelweiss Applied Science and Technology*, vol. 9, no. 4, pp. 1075-1087, 2025. <https://doi.org/10.55214/25768484.v9i4.6174>
- [44] G. Varga and V. Ferencsik, "Experimental examination of surface micro-hardness improvement ratio in burnishing of external cylindrical workpieces," *Cutting & Tools in Technological System*, no. 93, pp. 114-121, 2020. <http://dx.doi.org/10.20998/2078-7405.2020.93.13>
- [45] C. Felhö and G. Varga, "2D FEM investigation of residual stress in diamond burnishing," *Journal of Manufacturing and Materials Processing*, vol. 6, no. 5, p. 123, 2022. <https://doi.org/10.3390/jmmp6050123>
- [46] V. Kuznetsov *et al.*, "Normal force influence on smoothing and hardening of steel 03Cr16Ni15Mo3Ti1 surface layer during dry diamond burnishing with spherical indenter," *Metal Processing*, vol. 24, no. 1, pp. 6–22, 2022. <http://dx.doi.org/10.17212/1994-6309-2022-24.1-6-22>
- [47] J. Maximov and G. Duncheva, "The correlation between surface integrity and operating behaviour of slide burnished components—A review and prospects," *Applied Sciences*, vol. 13, no. 5, p. 3313, 2023. <https://doi.org/10.3390/app13053313>
- [48] I. Vuchkov and S. Stoyanov, "Mathematical modeling and optimization of technological objects," *Technika, Sofia*, p. 341, 1986.
- [49] I. N. Vuchkov and I. I. Vuchkov, *QStatLab Professional, v. 5.5 – statistical quality control software*. Sofia: User's Manual, 2009.
- [50] J. Maximov, G. Duncheva, A. Anchev, N. Ganey, and V. Dunchev, "Effect of cyclic hardening on fatigue performance of slide burnished components made of low-alloy medium carbon steel," *Fatigue & Fracture of Engineering Materials & Structures*, vol. 42, no. 6, pp. 1414-1425, 2019. <https://doi.org/10.1111/ffe.13001>
- [51] J. Maximov, A. Anchev, V. Dunchev, N. Ganey, G. Duncheva, and K. Selimov, "Effect of slide burnishing basic parameters on fatigue performance of 2024-T3 high-strength aluminium alloy," *Fatigue & Fracture of Engineering Materials & Structures*, vol. 40, no. 11, pp. 1893-1904, 2017. <https://doi.org/10.1111/ffe.12608>

- [52] G. Duncheva, J. Maximov, A. Anchev, V. Dunchev, and Y. B. Argirov, "Improvement in wear resistance performance of CuAl8Fe3 single-phase aluminum bronze via slide diamond burnishing," *Journal of Materials Engineering and Performance*, vol. 31, no. 3, pp. 2466-2478, 2022. <https://doi.org/10.1007/s11665-021-06389-6>
- [53] M. Korzynski, "Modeling and experimental validation of the force–surface roughness relation for smoothing burnishing with a spherical tool," *International Journal of Machine Tools and Manufacture*, vol. 47, no. 12-13, pp. 1956-1964, 2007. <https://doi.org/10.1016/j.ijmachtools.2007.03.002>
- [54] Ecoroll Catalogue, *Tools and solutions for metal surface improvement*. USA: Ecoroll Corporation Tool Technology, 2006.
- [55] K. Deb, A. Pratap, S. Agarwal, and T. Meyarivan, "A fast and elitist multiobjective genetic algorithm: NSGA-II," *IEEE Transactions on Evolutionary Computation*, vol. 6, no. 2, pp. 182-197, 2002. <https://doi.org/10.1109/4235.996017>